Exp Fluids (2017) 58:102
DOI 10.1007/s00348-017-2378-y

LETTER

An experimental study of icing control using DBD plasma actuator

Jinsheng Cai[1] · Yongqiang Tian[1] · Xuanshi Meng[1] · Xuzhao Han[1] · Duo Zhang[1] · Haiyang Hu[1]

Received: 7 April 2017 / Revised: 13 May 2017 / Accepted: 5 June 2017 / Published online: 7 July 2017

Abstract Ice accretion on aircraft or wind turbine has been widely recognized as a big safety threat in the past decades. This study aims to develop a new approach for icing control using an AC-DBD plasma actuator. The experiments of icing control (i.e., anti-/de-icing) on a cylinder model were conducted in an icing wind tunnel with controlled wind speed (i.e., 15 m/s) and temperature (i.e., −10 °C). A digital camera was used to record the dynamic processes of plasma anti-icing and de-icing whilst an infrared imaging system was utilized to map the surface temperature variations during the anti-/de-icing processes. It was found that the AC-DBD plasma actuator is very effective in both anti-icing and de-icing operations. While no ice formation was observed when the plasma actuator served as an anti-icing device, a complete removal of the ice layer with a thickness of 5 mm was achieved by activating the plasma actuator for ~150 s. Such information demonstrated the feasibility of plasma anti-/de-icing, which could potentially provide more effective and safer icing mitigation strategies.

Abbreviation

AC	Alternating current
DBD	Dielectric barrier discharge
F	Frequency of voltage source
n	Number of cycles
$P_{U.S}$	Power density per unit area
R	Activation period
S	Area wrapped by plasma actuator
t	Time of operation
T	Temperature
U_∞	Free-stream speed
$V_{\text{p-p}}$	Peak-to-peak voltage of voltage source
x, y, z	Axes of unwrapped actuator

✉ Xuanshi Meng
mxsbear@nwpu.edu.cn

[1] Northwestern Polytechnical University, Xi'an 710072, China

1 Introduction

Prevention of ice accretion on aerodynamic components has been a topic of great concern in the aerospace community. Ice may accumulate on all the exposed frontal surfaces of airplane or rotorcraft in flight which can significantly degrade the aerodynamic performance of airplane by decreasing lift and increasing drag. In wind energy, the ice accumulation on rotor blades has caused enormous overload threat on the tower, ice shedding hazard and power generation losses (Gent et al. 2000; Petty and Floyd 2004; Li et al. 2016).

Numerous methods have been developed and applied to mitigate the icing effects on aircraft and wind turbine operations. These methods fall into two distinct categories: (1) anti-icing (i.e., ice prevention) and (2) de-icing (i.e., ice removal). Anti-icing approaches are used to prevent ice formation from the protected areas, whereas de-icing methods are usually performed to remove ice after a certain amount has accumulated. In general, the methods can also be classified into three categories (Pourbagian et al. 2014; Thomas et al. 1996): (1) the liquid-based, such as weeping wings; (2) the mechanical-based, such as pneumatic boots, and (3) thermal-based, such as hot air (Pellissier et al. 2010; Dong et al 2015) and electro-thermal systems (Pourbagian et al. 2014).

With respect to performance optimization, the majority of current anti-/de-icing systems were, however, developed without considering the potential aerodynamic degradation. In order to improve the operational performance of aircraft/

wind turbine in cold weather, methods and techniques for more efficient anti-/de-icing performance are considered desirable (Parent and Ilinca 2011; Nagappan et al. 2013; Pourbagian et al. 2014; Liu et al. 2017a, b).

As an active flow control technique, plasma flow control has received growing research attention in recent years because of the advantages of non-mechanical parts, zero reaction time, broad frequency bandwidths and relatively low energy consumption. Most importantly, the plasma actuators can be conveniently arranged on the surface of the vehicle parts. One such development is the use of dielectric barrier discharge (DBD) plasma actuators driven by an alternating current (AC) source. The AC-DBD plasma actuator for aerodynamic flow control is composed of two electrodes separated by one dielectric material arranged in an asymmetric fashion. Application of a sufficiently high-voltage AC signal between the electrodes causes the air over the covered electrode to ionize. The ionization of the air is a dynamic process within the AC cycle. The ionized air, in the presence of the electric field, results in a body force vector that acts on the ambient air. Such controlled body force can be modulated to achieve active aerodynamic control (Moreau 2007; Corke et al. 2008; Little and Samimy 2010).

For DBD actuator, the electrons gain energy from an external electric field and transfer this energy through collisions into the various degrees of freedom of other particles; most of this energy is eventually released as heat (Aleksandrov et al. 2010). Thus, in addition to aerodynamic effect, the AC-DBD plasma actuator also has a thermal effect on the electrode sheet, the substrate, and the surrounding air during the high-voltage discharge, which has been observed in previous studies (Joussot et al. 2010; Stanfield and Menart 2009; Dong et al. 2008; Jukes et al. 2007; Kotsonis et al. 2014; Erfani et al. 2012). Joussot et al. (2010) have revealed a rapid and significant linear increase of the dielectric temperature on the order of 50 °C after ignition of the discharge by using an infrared imaging technique. Stanfield and Menart (2009) reported the spatially resolved rotational and vibrational temperatures for a dielectric barrier discharge (DBD) by emission spectroscopy. The results indicated that the maximum rotational temperature in the DBD is 137 °C, which is located at the interface between the exposed and buried electrode, while the minimum value of the temperature measured was 37 °C located at the edge of the discharge region. Dong et al. (2008) also used a thermocouple to measure the temperature of the dielectric panel versus the operation time. A relatively linear increase in temperature of ~70 °C was observed after running the actuator for 14 min.

In terms of implementations of AC-DBD for icing mitigation on aircraft and wind turbines, the unique features of DBD (i.e., zero reaction time, non-mechanical parts and low energy consumption) are preferable for a potentially efficient and safer anti-/de-icing operations. As a sophisticated approach for leading-edge flow control, the installation of DBD is usually located at the icing-susceptible stations. The excitation of plasma can not only prevent hazard ice accretion around the leading edge, but also facilitate the aerodynamic performance as a flow control approach. In comparison to the conventional heating element, the AC-DBD plasma actuator has the potential to generate heat both at the ice--substrate interface and in the ice structures, especially for rime ice with air bubbles trapped inside.

This study demonstrates the use of an AC-DBD plasma actuator fabricated to serve as an anti-/de-icing device. A feasibility study of plasma anti-/de-icing on a cylinder model was conducted in an icing wind tunnel with controlled wind speed and temperature. In the text that follows, the details of plasma anti-/de-icing methodologies are illustrated at first. Then, the anti-/de-icing performance of the AC-DBD plasma actuator is evaluated based on visualization and thermal images. A power consumption analysis of the plasma de-icing operations is also performed to provide essential concepts for comparison with the conventional thermal approaches.

2 Experimental setup

Plasma anti-/de-icing experiments are conducted in a closed-circuit low-speed icing wind tunnel as shown in Fig. 1. The test section of the icing wind tunnel has a cross section of 0.3 m in width and 0.5 m in height. The icing wind tunnel has the capacity of generating airflow velocity ranging from 5 to 18 m/s, and the air temperature from −25 to 30 °C. An electric heater is used to generate supercooled water droplets (50–200 μm in size), which corresponds to large droplets as defined in Nagappan et al. (2013). The liquid water content (LWC) in the icing wind tunnel could be adjusted from 0.5 to 1.0 g/m^3.

In the present study, a cylinder model made of Teflon is manufactured and used for icing test. The cylinder model has a diameter of 45 mm, and a length of 220 mm as shown in Fig. 2a. The set AC-DBD plasma actuator is fabricated with six exposed electrodes and seven encapsulated electrodes separated by a dielectric layer (i.e., Kapton film), as shown in Fig. 2b. These actuators are closely attached on the cylinder surface with an effective length of 80 mm, the rest of model is with no-plasma actuator. The different length of plasma actuator and complete model is in order to show the difference of ice accumulation with and without icing control. Each individual plasma actuator is composed of two copper electrodes with the same thickness of 0.03 mm, and a Kapton dielectric film with a thickness of 0.33 mm. The two copper electrodes are of different width

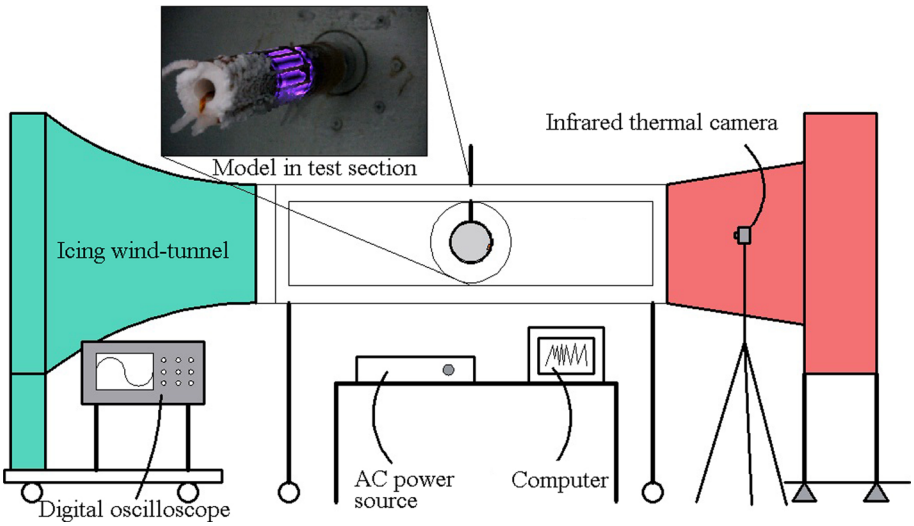

Fig. 1 Schematic illustration of the de-icing and anti-icing tests in the icing wind tunnel (only the test section is given)

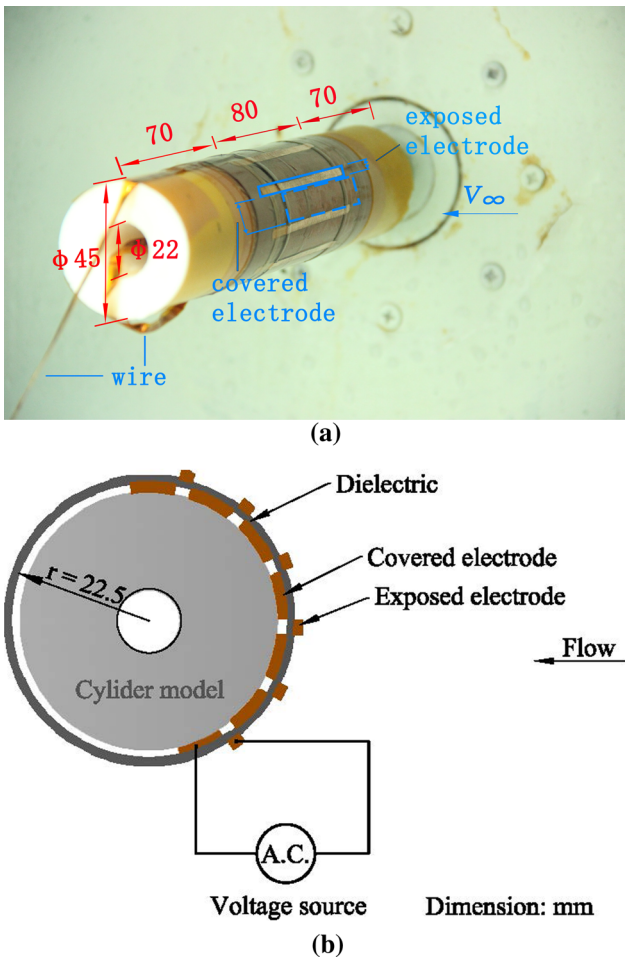

Fig. 2 Model set in the icing wind tunnel and schematic illustration of the plasma actuator. **a** Model with plasma actuator. **b** Multi-electrode actuator.

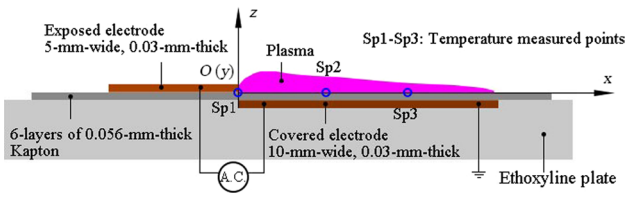

Fig. 3 Schematic illustration of the unwrapped DBD actuator geometry

dimensions (i.e., with the exposed and the encapsulated electrodes being 3.3 and 10 mm, respectively), and asymmetrically separated by the Kapton film. There is no gap or overlap between the exposed and encapsulated electrodes for the actuator configuration in the present study. A schematic of the AC-DBD plasma actuator along with the measurement coordinates is shown in Fig. 3.

The actuators are connected to a high-voltage AC source (model CTP-2000K by Nanjing Suman Co.) that provides a peak-to-peak amplitude of $V_{p\text{-}p} = 0$–30 kV, and a center frequency of $f = 1$–100 kHz. The voltage and current output to the actuator are measured by a Tektronix P6015A high-voltage probe. The current through the actuator is measured by a Pearson Electronics model 2877 AC current probe. The voltage and current signals are displayed and processed with a Tektronix DPO3054 oscilloscope.

Surface temperature measurements are obtained by using an FLIR Systems T660 infrared (IR) camera, which has an accuracy of $+/-2$ °C at room temperature. The wavelength range that can be detected by the camera sensor is from 7.5 to 14 μm. The measurement range of the IR camera is -40 to 650 °C. The camera has a resolution

of 640 × 480 pixels, and the video frame rate is 30 Hz. The working distance of the camera is 500 mm with a 400 mm × 30 mm field of view. The plasma is only generated within the region over the covered electrode, therefore, the temperature distribution over the covered electrode is studied. Three temperature reading points are chosen at the 50% span of the actuator, as clearly shown in Fig. 3 and Table 1.

The camera recorded the infrared emission of the dielectric surface which is a function of its temperature. The surface emissivity of the Kapton is used to calculate the temperature, which is set at 0.83 (Tomohiro Okada 2016). The surface temperature of the exposed electrode, made of copper, is not given in this study due to the different surface emissivity. Other parameters, including the working distance of the camera, the static temperature in test section and its relative humidity are also considered for the temperature calculation.

In this study, an icing environment was first created by the icing wind tunnel with the airflow velocity and temperature being set at 15 m/s and −10 °C, respectively. The Reynolds number is 57,700 based on the diameter of the cylinder. After a few cycles of stabilization of the wind tunnel parameters (i.e., airflow velocity and temperature), the spray system was manipulated to generate the desired droplet size and LWC for icing tests.

Table 1 The reading point coordinates of the surface temperature measurements on the unwrapped plasma actuator, 50% span

Points	Sp1	Sp2	Sp3
x (mm)	0	3.0	6.0

3 Results

3.1 Anti-icing study in icing wind tunnel

For the anti-icing test at the icing wind tunnel, the plasma was activated after water vapor had been sprayed for ~5 s. The time was set at the beginning of the plasma actuation. As the plasma actuator was activated, a high-voltage field was generated between the exposed electrode and encapsulated electrode, which ionized the air over the dielectric layer (i.e., Kapton film). The existence of such dielectric barrier leads to a large volume of plasma that is generated in preventing the discharge collapsing into an arc. Since there is no closed-circuit between the exposed and encapsulated electrodes, the appearance of water and ice would not make a short circuit as long as the dielectric layer is well functioned (Falkenstein and Coogan 1997).

Figure 4 shows the anti-icing process by plasma actuation for $V_{p\text{-}p} = 15.0$ kV and $f = 13.4$ kHz at 0–930 s time duration. It demonstrates that the plasma actuator is able to withstand the discharge without breaking down during the test. With 5-s water vapor spraying, the leading edge of the model is covered by a thin layer glaze ice. The plasma glow first appears in the

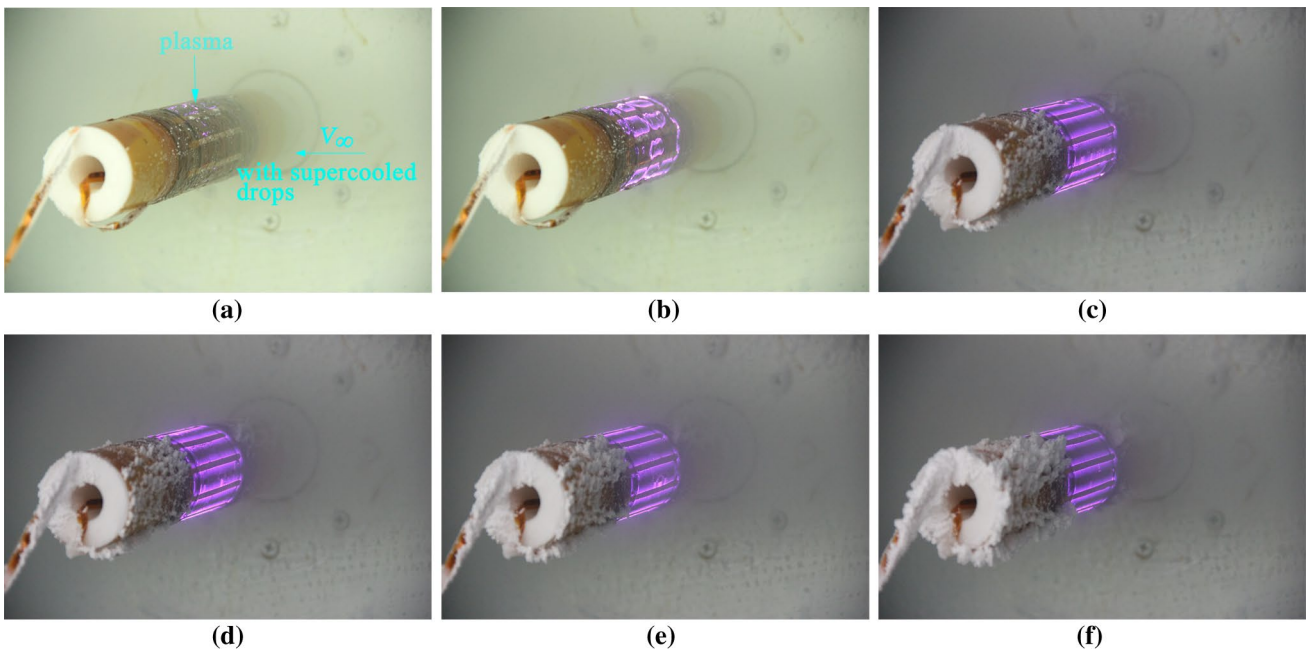

Fig. 4 Process of AC-DBD plasma anti-icing for the multi-actuator model for $V = 15$ m/s and $T = -10$ °C. **a** $t = 0$ s. **b** $t = 30$ s. **c** $t = 210$ s. **d** $t = 450$ s. **e** $t = 690$ s. **f** $t = 930$ s.

region back to the leading edge where there is the thinner ice layer, as shown in Fig. 4a. The glow of the plasma shows the discharge area is limited by the ice layer and changes with the plasma duration, as shown in Fig. 4a–c. After about 30 s discharge, the glow of the plasma becomes even.

With the plasma actuation, the flow and temperature conditions of the model surface have changed. When the supercooled water droplets impact the model, they do not change state from liquid to ice, instead they remain liquid due to absorption of the heat of discharge. Such liquid water can affect the plasma distributions when it flows past the discharge region, as shown in Fig. 4d. After 16 min of plasma actuation, no ice accretion occur on cylinder surface in the region of plasma actuators, whereas the clear (glaze) ice is formed at the stagnation region bordered by rime ice in the no-plasma actuation region. This demonstrates that the plasma actuation has a very clear anti-icing effect.

3.2 De-icing study in icing wind tunnel

In the de-icing test, the wind tunnel firstly ran with the spray of the supercooled drops for 15 min, followed by turning the drop spray off, then the plasma was activated at a voltage of 15.0 kV and a frequency of 13.4 kHz with the constant airspeed and temperature. Figure 5 shows the de-icing process with the test photos at the different operation times. A combination of rime and glaze ice is formed with an average thickness of 5 mm on the leading edge of the cylinder, as shown in Fig. 5a. The glaze ice accretes around the stagnation line of the cylinder, while the rime ice forms downstream and nearby the glaze ice. Such ice structure was also observed in the study of Hansman and Kirbyti (1986).

During plasma actuation, the glow first appears in the region where there is less ice accretion, as shown in Fig. 5a, b, because there is enough air to be discharged. This is essential for the DBD plasma under atmospheric conditions. The discharge then appears in the rime ice region, as shown in Fig. 5c, d. The rime ice always traps air molecules inside because of sudden freezing at extremely low temperatures, consequently, a soft and loose structure was observed. Therefore, the plasma discharge occurs on the surface of the model and in the space inside the ice layer. The clear ice eventually melts due to the cohesive and dense structure. After a few seconds, the ice melts at all of the discharge regions; the ice decreases and no longer accretes on the surface of the cylinder like the anti-icing process. After the plasma actuated for 150 s, the ice layer is completely removed from the surface of the cylinder as shown in Fig. 5e, f.

3.3 De-icing power consumption

De-icing control is a process in which interfacial ice attached to a structure is either broken or melted, so only a thin layer of interfacial ice needs to be melted. The ice is then removed due to wind shear.

The lowest voltage required to make the surface temperature of the actuator greater than 0 °C is sought in order to determine the minimum energy input for de-icing. Figure 6 shows the infrared images of the de-icing process for the multi-actuator model at different voltages. The surface temperature distribution along the chord of the covered electrode at 50% span, located in the region of the rime ice accretion is studied. The exposed electrode is masked by the brown color. The infrared image for the plasma off

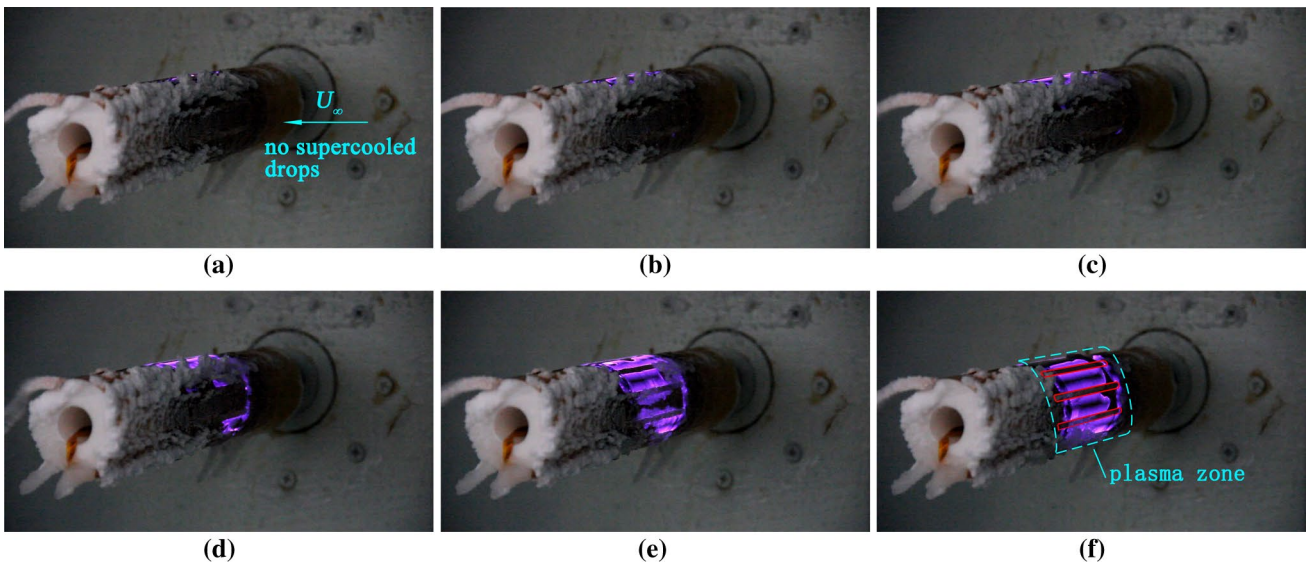

Fig. 5 Process of AC-DBD plasma de-icing for the multi-actuator model $V = 15$ m/s and $T = -10$ °C. **a** $t = 30$ s. **b** $t = 60$ s. **c** $t = 90$ s. **d** $t = 120$ s. **e** $t = 150$ s. **f** $t = 180$ s.

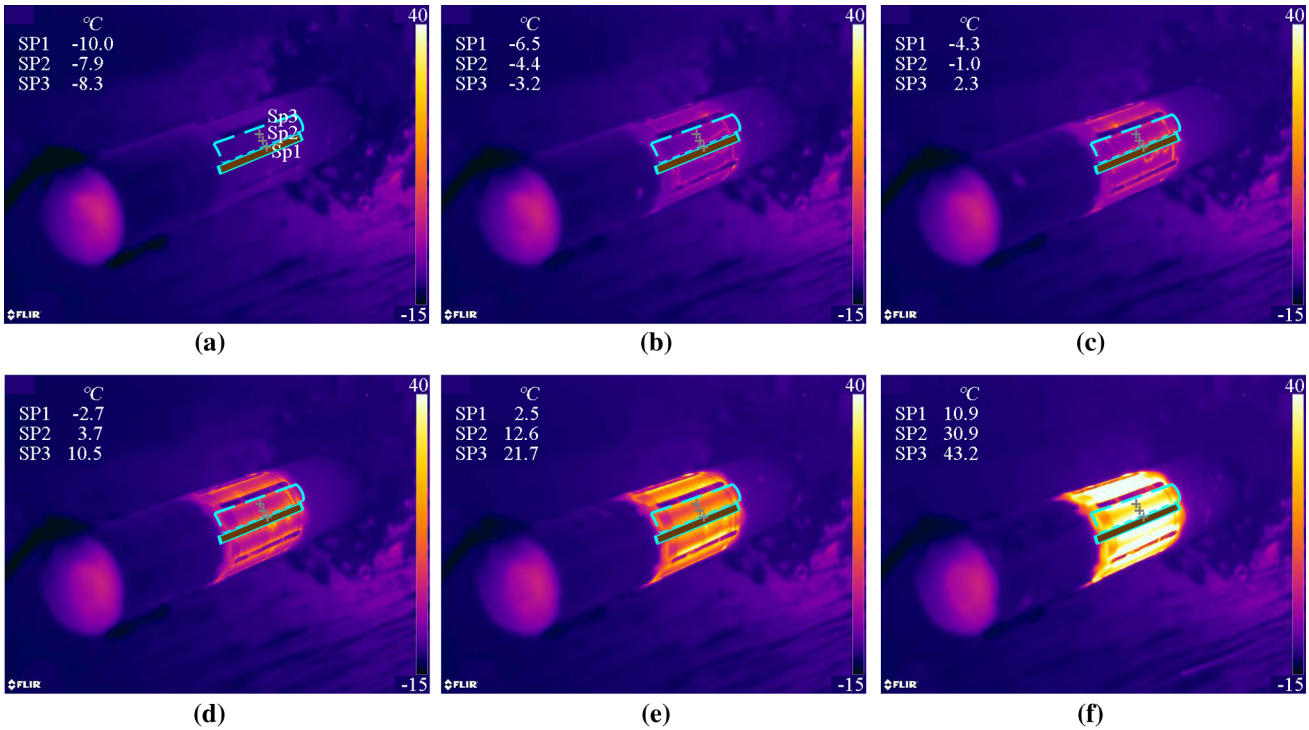

Fig. 6 Thermal image of AC-DBD plasma of the multi-actuator model with different voltages at different times in the icing wind tunnel. **a** $t = 0$ s, $V_{p\text{-}p} = 0$. **b** $t = 25$ s, $V_{p\text{-}p} = 6.3$ kV. **c** $t = 50$ s, $V_{p\text{-}p} = 8.0$ kV. **d** $t = 100$ s, $V_{p\text{-}p} = 10.0$ kV. **e** $t = 130$ s, $V_{p\text{-}p} = 12.0$ kV. **f** $t = 160$ s, $V_{p\text{-}p} = 14.0$ kV

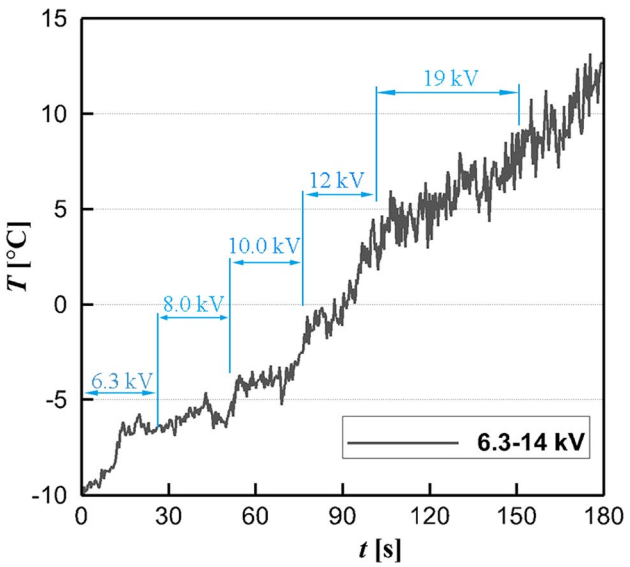

Fig. 7 Surface temperature distribution and excitation voltage of AC-DBD for the multi-actuator model in the de-icing test (Sp1)

with a flowfield temperature of −10 °C is shown in Fig. 6a, it can be seen that the temperature distribution is not even with the uneven ice accretion.

As shown in Fig. 6b–f, the surface temperature of the actuator increases with increasing voltages and the time durations. The temperature changes with the voltage at $x = 0$ (Sp1) is presented in Fig. 7; six voltage values are evaluated with a fixed frequency of 11.5 kHz. The voltage continuously increases during the test. For each fixed voltage, the duration is ~30 s. For $V_{p\text{-}p} = 6.3$ kV, the surface temperature of the discharge zone is below 0 °C. When the voltage is increased to 12.0 kV, the surface temperature is greater than 0 °C and the area of the plasma glow significantly increases. The surface temperature variation with the voltages is almost linear.

The active power consumption is measured as a function of the amplitude of the applied voltages at the constant frequency, $F = 13.4$ kHz. The power density per unit area, $P_{U.S}$, for the de-icing test is shown in Fig. 8. This value is calculated using Eq. (1), where R, n, S denote the activation period, the number of cycles and the area wrapped by plasma actuators, respectively. As discussed above, the surface temperature becomes higher than 0 °C at 12.0 kV for the multi-actuator model during the de-icing test; at this voltage, the power density is ~13 kW/m^2.

$$P_{U.S} = \frac{1}{nR.S}\int_{nR} V(t).I(t)dt \tag{1}$$

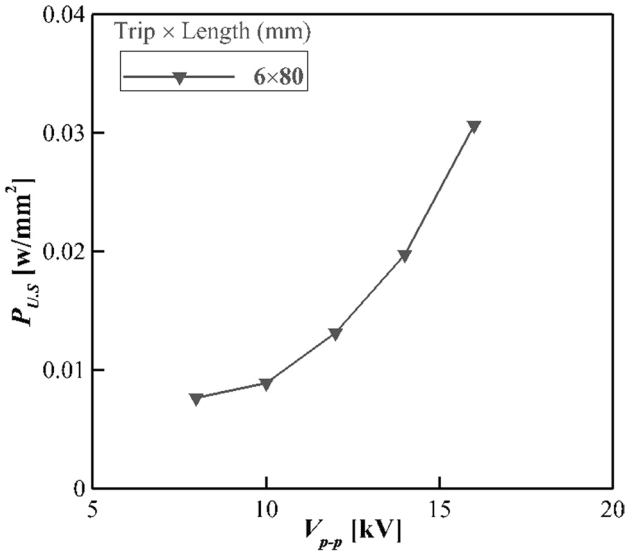

Fig. 8 Power density at different voltages for the de-icing test

It should be noted that the temperature maps are being compared to two controllable variables, voltages and the time durations, in the de-icing power consumption study. This method is crude as it is difficult to isolate the effect of $V_{\text{p-p}}$ if the time duration is changing, and vice versa. A careful power consumption study of the plasma icing control is required for further work.

4 Conclusions

Icing control on a cylinder in the icing wind tunnel has been demonstrated by employing an AC-DBD plasma actuator at the leading edge of the cylinder model. The mixed structural ice forms on the leading edge when the model is subjected to the supercooled flow with the large droplets. The results show that the mixed ice layer can be completely removed from the model surface after a few minutes of plasma actuation in the de-icing test. In anti-icing test, plasma actuation can completely prevent ice formation on the surface of the cylinder model. Power consumption results show that the plasma actuation has a relatively low power consumption. The introduced plasma icing control approach appears to be highly promising and it will be further investigated. For instance, future work may investigate the mechanism for plasma de-icing and anti-icing. The optimization of plasma actuator, including the dielectric barrier material, the geometric and electronic parameters will be studied. Furthermore, the current study could be extended to include airfoil and nacelle geometries and used to examine their de-icing and anti-icing performances for realistic configurations.

Acknowledgements This work is supported by the National Natural Science Foundation of China (Grant Nos. 11472221 and 11672245), the National Key Laboratory Research Foundation of China (Grant No. 9140C420301110C42) and the 111 Project (B17037).

References

Aleksandrov NL, Kindysheva SV, Nudnova MM, Starikovskiy AY (2010) Mechanism of ultra-fast heating in a non-equilibrium weakly ionized air discharge plasma in high electric fields. J Phys D Appl Phys 43:1–19

Choi K-S, Segawa T, Yoshida H (2007) Jet flow induced by a surface plasma actuator. Proc Inst Mech Eng Part I 222:347–356

Corke TC, Post ML, Orlov DM (2008) Single-dielectric barrier discharge plasma enhanced aerodynamics: concepts, optimization, and applications. J Propuls Power 24:935–945

Dong B, Bauchire JM, Pouvesle JM, Magnier P, Hong D (2008) Experimental study of a DBD surface discharge for the active flow control of subsonic airflow. J Phys D Appl Phys 41:1–9

Erfani R, Behtash HZ, Kontis K (2012) Plasma actuator: influence of dielectric surface temperature. Exp Therm Fluid Sci 42:258–264

Falkenstein Z, Coogan JJ (1997) Microdischarge behaviour in the silent discharge of nitrogen-oxygen and water-air mixtures. J Phys D Appl Phys 30:817–825

Gent RW, Dart NP, Cansdale JT (2000) Aircraft icing. Philos Trans R Soc A Math Phys Eng Sci 358:2873–2911

Hansman RJ, Kirbyti MS (1986) Measurement of ice growth during simulated and natural icing conditions using ultrasonic pulse-echo techniques. J Aircr 23:492–498

Joussot R, Hong D, Rabat H, Boucinha V, Weber-Rozenbaum R, Chesneau AL (2010) Thermal characterization of a dbd plasma actuator: Dielectric temperature measurements using infrared thermography. AIAA Paper 2010-5102

Li H, Rye MW, Hu H (2016) An experimental investigation on unsteady heat transfer and transient icing process upon impingement of water droplets. AIAA Paper 2016-0510

Little J, Samimy M (2010) High-lift airfoil separation with dielectric barrier discharge plasma actuation. AIAA J 48:2884–2898

Liu L, Bond J, Hu H (2017a) Ultrasonic-attenuation-based technique for ice characterization pertinent to aircraft icing phenomena. AIAA J 55:1602–1609

Liu Y, Chen W, Bond LJ, Hu H (2017b) An experimental study on the characteristics of wind-driven surface water film flows by using a multi-transducer ultrasonic pulse-echo technique. Phys Fluids 29:012102 (1–13)

Moreau E (2007) Airflow control by non thermal plasma actuators. J Phys D Appl Phys 40:605–636

Nagappan N, Golubev VV, Habashi W (2013) Parametric analysis of icing control using synthetic jet actuators. AIAA Paper 2013-2453

Okada TSA, Ishige R (2016) Analysis of thermal radiation properties of polyimide and polymeric materials based on atr-ir spectroscopy. J Photopolym Sci Technol 29:251–254

Parent O, Ilinca A (2011) Anti-icing and de-icing techniques for wind turbines: critical review. Cold Reg Sci Technol 65:88–96

Pellissier M, Habashi WG, Pueyo A (2010) Design optimization of hot-air anti-icing systems by fensap-ice. AIAA Paper 2010-1238

Petty KR , Floyd CDJ (2004) A statistical review of aviation airframe icing accidents in the US. National Transportation Safety Board

Pourbagian M, Talgorn B, Habashi W, Kokkolaras M, Digabel SL (2014) On power optimization of aircraft electro-thermal anti-icing systems. G-2014-72

Stanfield SA, Menart J (2009) Rotational and vibrational temperature distributions for a dielectric barrier discharge in air. AIAA J 47:1107–1115

Thomas SK, Cassoni RP, MacArthur CD (1996) Aircraft anti-icing and de-icing techniques and modeling. J Aircr 33:841–854

Winkel R, Correale G, Kotsonis M (2014) Effect of dielectric material on thermal effect produced by ns-DBD plasma actuator. AIAA Paper 2014-2119

Zheng M, Chen Y (2015) Thermal analysis and testing of nonrotating cone with hot-air anti-icing system. J Propuls Power 31:896–903